King Saud University

Arabian Journal of Chemistry

www.ksu.edu.sa
www.sciencedirect.com

ORIGINAL ARTICLE

Amelioration of human acute lymphoblastic leukemia (ALL) cells by ZnO-TiO₂-Chitosan-Amygdalin nanocomposites

Abozer Y. Elderdery [a,b,*], Badr Alzahrani [a], Fehaid Alanazi [c], Siddiqa M.A. Hamza [d], Ahmed M.E. Elkhalifa [e,f], Abdulaziz H. Alhamidi [g], Abdulrahim A. Alabdulsalam [h], A. Mohamedain [h,i], Suresh S. Kumar [j], Pooi Ling Mok [k]

[a] Department of Clinical Laboratory Sciences, College of Applied Medical Sciences, Jouf University, Sakaka, Saudi Arabia
[b] Health Sciences Research Unit, Jouf University, Sakaka, Saudi Arabia
[c] Department of Clinical Laboratory Sciences, College of Applied Medical Sciences-AlQurayyat, Jouf University, Saudi Arabia
[d] Department of Pathology, Umm Alqura University, Algunfuda, Saudi Arabia
[e] Department of Public Health, College of Health Sciences, Saudi Electronic University, Riyadh, Saudi Arabia
[f] Department of Haematology, Faculty of Medical Laboratory Sciences, University of El Imam El Mahdi, Kosti, Sudan
[g] Clinical Laboratory Sciences Department, College of Applied Medical Science, King Saud University, Riyadh, Saudi Arabia
[h] Department of Biomedical Sciences, College of Medicine, King Faisal University, Alhofuf, Saudi Arabia
[i] Department of Biochemistry, Faculty of Medicine, Khartoum University, Sudan
[j] Centre for Materials Engineering and Regenerative Medicine, Bharath Institute of Higher Education and Research, Chennai, India
[k] Department of Biomedical Science, Faculty of Medicine & Health Sciences, Universiti Putra Malaysia, 43400 UPM Serdang, Selangor, Malaysia

Abstract The present study aims to study the cytotoxicity of ZnO-TiO₂-Chitosan-Amygdalin nanocomposites (ZnO-TiO₂-Chitosan-Amygdalin) on T lymphoblast cancer cells (MOLT-4). In a study, nanocomposites containing 2.5 to 15 μg/ml MTT were screened for their anticancer activity. Its anticancer properties were significantly higher than those of other nanocomposites with an IC_{50} value of 10.34 μg/ml. We studied the mechanism of action for cytotoxic cell death by fluorescence microscopy using Acridine Orange/EtBr (AO/EtBr) and Rhodamine 123 staining procedures. Using

* Corresponding author at: Department of Clinical Laboratory Sciences, College of Applied Medical Sciences, Jouf University, Sakaka, Saudi Arabia.
 E-mail address: ayelderdery@ju.edu.sa (A.Y. Elderdery).
Peer review under responsibility of King Saud University.

Production and hosting by Elsevier

DCFH-DA, ZnO-TiO$_2$-Chitosan-Amygdalin nanocomposites were analyzed to determine ROS production. The change in apoptotic protein expression for the 24 h following treatment with MOLT-4 cells for Caspase-3, 8, and 9. Nanocomposites containing ZnO-TiO$_2$-Chitosan-Amygdalin increased the number of early and late apoptotic cells in MOLT-4 cells. ZnO-TiO$_2$-Chitosan-Amygdalin nanocomposites also enhanced mitochondrial apoptosis through Caspase cascade signaling. MOLT-4 cells phosphorylated Caspase cascade in response to ZnO-TiO$_2$-Chitosan-Amygdalin nanocomposites. Compared to the control group, the cancer cells treated with ZnO-TiO$_2$-Chitosan-Amygdalin nanocomposites significantly arrest the proliferation and induces cleavage of pro-apoptotic proteins which leads to apoptotic cell death. Accordingly, ZnO-TiO$_2$-Chitosan-Amygdalin nanocomposites might be effective against T lymphoblast cancer.

1. Introduction

Acute lymphoblastic leukemia (ALL) results from abnormal white blood cells that begin to grow in your bone marrow, which is the soft, inner part of your bones. The immune system relies on these white blood cells, which develop from immature lymphocytes (Chang et al., 2021; Terwilliger and Abdul-Hay, 2017). The most common childhood cancer is acute lymphoid leukemia, which peaks between 2 and 5 years of age (Kato and Manabe (2018)). The cure rate for this disease has increased to over 90% due to improved management and treatment, but disease relapse and resistance to treatment persist as significant clinical challenges (Balsat et al., 2020). When combined cytotoxic chemotherapy is used to treat ALL, most adults and about 20% of children relapse within five years (Inaba and Mullighan, 2020). The identification of the genes and biological pathways responsible for chemoresistance is essential to the development of new therapeutic approaches to improve patient survival. The prevalence of ALL in children is about 80%, but in adults, it is a devastating disease (Inaba and Pui, 2021). A report from the National Cancer Institute estimates that ALL is found in 1.6 out of every 100 000 Americans. According to the American Cancer Society, more than 1400 deaths were linked to ALL in 2016 (Siegel et al., 2021). All types of leukemia appear to be distributed bimodally, with a peak in childhood and another peak around the age of 50. After dose intensification strategies, pediatric outcomes have significantly improved, but the elderly continue to have a very poor prognosis (Dai et al., 2021). Although induction chemotherapy is very successful in remission adult patients with ALL, only 30–40% of these patients will live for more than five years (Jung et al., 2010).

Many physicians diagnose the patient with locally advanced or metastatic disease due to the lack of distinctive symptoms in the early stages and the lack of available biomarkers (Aberuyi et al., 2020). To improve the clinical prognosis of ALL patients, more effective strategies for early detection and more effective treatment options are necessary. A significant challenge in ALL research is not only the fact that it is a rare tumor, but also the difficulty in obtaining human tissue samples and the lack of experimental models. Current cancer treatments use alkylating agents and antimetabolites, which can have adverse effects and are notorious for causing systemic toxicity. Among the most cutting-edge methods in cancer treatment is the use of nanomaterials and nanostructured devices to deliver anticancer medications (Javed et al., 2020).

A variety of industries use Chitosan, including food, textiles, agriculture, water treatment, cosmetics, and pharmaceuticals. In addition to its biodegradability and non-toxicity, it also has antimicrobial properties that make it an effective wound healing agent. The use of chitosan in combination with zinc oxide (ZnO), titanium dioxide (TiO$_2$), and silver nanoparticles (NPs) is essential to improve its performance (Bui et al., 2017; Tatarinov et al., 2021). The use of metal nanocomposites in cancer biology is being investigated for diagnostic and therapeutic purposes. A variety of chemical functional groups can be used to alter metal and metal oxide nanocomposites as necessary (Kustiningsih

et al., 2019). Recently, a lot of attention has been paid to ZnO-TiO$_2$-Chitosan-Amygdalin nanoparticles as a potential cancer treatment. In particular, the underlying mechanisms of ZnO-TiO$_2$-Chitosan-Amygdalin-induces apoptosis in cancer cells have not been explored due to the lack of ZnO-TiO$_2$-Chitosan-Amygdalin treatment. In this study, we performed the anti-cancer activity of human ALL cancer cell lines using ZnO-TiO$_2$-Chitosan-Amygdalin nanocomposites.

2. Material and methods

2.1. Chemicals

We purchased zinc oxide dispersion, sodium alginate, and polyethylene glycol from Sigma Aldrich in the USA, and an Amygdalin compound also from Sigma Aldrich in the USA.

2.2. Synthesis of ZnO-TiO$_2$-Chitosan-Amygdalin nanocomposites

The chemical precipitation process synthesized ZnO-TiO$_2$-Chitosan-Amygdalin. In an aqueous medium, 0.1 M of zinc (NO$_3$)$_2$ 6H$_2$O was added with 500 mg of TiO$_2$ NPs, and 500 mg of chitosan was dissolved in 50 mL of 1% acetic acid. A 50 mg phytocomponent solution of Amygdalin in ZnO-TiO$_2$-Chitosan is added to this. In the end, the white residue was obtained by dropping 0.1 M of NaOH solution into the ZnO-TiO$_2$-Chitosan-Amygdalin solution several times. An electric stirrer was used to heat the residue for 3 h at room temperature. Different times of deionized water and ethanol solutions were used to wash the obtained Nanopowder. After centrifugation for 40 min at -3 °C, the resultant solution was centrifuged at 15,000 rpm for 15 min. This was followed by 2 h of drying at 200 °C.

2.3. The characterization of ZnO-TiO$_2$-Chitosan-Amygdalin nanocomposites:

2.3.1. Fourier transform infrared analysis

FTIR spectroscopy was conducted to study the ZnO-TiO$_2$-Chitosan-Amygdalin nanocomposites for possible reducing agents. Following the drying of the ZnO-TiO$_2$-Chitosan-Amygdalinnanocomposites powder, they were powdered and pelletized, and the spectra were measured in diffuse reflectance mode using Perkin-Elmer spectra (wavelength range between 4000 cm^{-1} and 400 cm^{-1}).

2.3.2. Photographic luminescence spectroscopy (PLS)

Fluorescence spectrophotometers were used to obtain photoluminescence spectra. Eclipse (Varian) using a slit width of 5 nm, the scan rate of 120 nm/min, the interval of 1 nm (average time 0.5 s), the voltage of 600 V, and wavelength of 325 nm of excitation. A time-resolved photoluminescence technique was performed using a laser coupled to an optical parametric oscillator (OPO) at a frequency of 10 Hz to excite the sample at 325 nm. ICCD Instaspec V ICCD detector and Hg lamp calibration were used to analyze the sample emission with an Oriel f-125 monochromator graded at 400 grooves/mm.

2.4. Measuring SEM with EDAX

An XL 30 Philips scanning electron microscope was used to examine the structure of the $ZnO-TiO_2$-Chitosan-Amygdalin nanocomposites, and an Inspect 50 FEI microscope was used for high-resolution scanning electron microscopy (FEG-SEM). To prepare the SEM samples, $ZnO-TiO_2$-Chitosan-Amygdalin nanocomposites were dispersed in isopropyl alcohol, then drop coated on Al2O3, and then dried in an oven at 80 °C for 30 min. ZEISS GeminiSEM was used to analyze the nanocomposites film.

2.5. Dynamic light scattering (DLS) and X-ray diffractive imaging

The $ZnO-TiO_2$-Chitosan-Amygdalin nanocomposites were analyzed using an XRD diffractometer with a copper tube mounted on a Bruker D8 Advance. We used DIFFRAC and EVA V3.1 to analyze our diffractograms, and the COD2013 (Cristallography Open Data − 2013) database to analyze the data. We calculated the crystal size based on the XRD results using the Scherrer equation. Based on Brownian motion, the size distribution of $ZnO-TiO_2$-Chitosan-Amygdalin nanocomposites was evaluated using the dynamic light scattering (DLS) technique and a Malvern ZEN3600 Zetasizer. Following dissolving 1 mg of $ZnO-TiO_2$-Chitosan-Amygdalin nanocomposites particle, a stir was performed for 2 min using the Ultronique disruptor ultrasonic probe. The solution was vortexed for 15 min, ultrasonically (25 kHz), and ultrasonically (25 kHz) for 15 min.

2.6. Cell culture of MOLT-4 cells

Using a Human MOLT-4 cell line obtained from the ATCC, USA, we cultured them in 10% FBS and Eagle's Minimum Essential Medium containing 1% penicillin–streptomycin. Incubation of the cells at 37 °C was accompanied by CO_2 addition of 5% every 48 h. The experiments were performed with cells subcultured at 80% confluency using a trypsin-EDTA solution with 0.25 percent trypsin.

2.7. MTT assay

MOLT-4 cells were seeded and exposed to 5% CO_2 for 24 h before plating into 96-well plates. Different concentrations of $ZnO-TiO_2$-Chitosan-Amygdalin nanocomposites were applied to the cells after 24 h of incubation (2.5, 5, 7.5, 10, 12.5, and 15 μg/ml). An MTT assay was performed on the cells, and the medium was discarded. We incubated the cells at 37 °C in the dark for 3 h after adding a serum-free culture medium to each well. After adding the 150 μl MTT solution to each well after incubation, plates were wrapped in foil and shook for 15 min. A UV spectrophotometer from Shimadzu was used to measure the optical density of the solution at 595 nm and calculate the percentage of viable cells (Subbarayan et al., 2016).

2.8. ROS staining

DCFH-DA staining was performed using 24 well plates in our cell culture system. Incubation with $ZnO-TiO_2$-Chitosan-Amygdalin nanocomposites in 7.5 and 10 μg/ml concentrations at 37 °C in 5% CO_2 was followed by 24 h of incubation. Following incubation with DCFH-DA stain, 30 min were required for staining with this stain. Using an fluorescence microscope (Labomed, USA), we examined the cells twice in PBS to seek out the fluorescent emitters.

2.9. Rhodamine-123 staining

$ZnO-TiO_2$-Chitosan-Amygdalin nanocomposites treated and untreated cells were compared for mitochondrial membrane permeability using Rhodamine 123 staining. To 24 well plates containing MOLT-4 cells, 7.5 and 10 μg/ml of $ZnO-TiO_2$-Chitosan-Amygdalin nanocomposites were added. Incubation of the cells was completed after incubating them for 30 min with 1mMol Rhodamine 123 after twice rinsing them in PBS. The stained cells were viewed under a fluorescence microscope (Labomed, USA) after 15 min of incubation in the dark.

2.10. Acridine orange/ethidium bromide staining (AO/EtBr)

Nanocomposites used double staining, AO/EtBr, induced the death of human acute lymphoblastic leukemia (ALL). We incubated MOLT-4 cells at 37 °C alongside $ZnO-TiO_2$-Chitosan-Amygdalin nanocomposites (7.5 and 10 μg/ml) solutions for 24 h. After washing the cells with PBS, the cells were stained with Acridine Orange and Ethidium Bromide (1:1). The cells were examined under a fluorescence microscope (Labomed, USA), stained cells were examined after 30 min of incubation in the dark.

2.11. Caspase-3, 8, and 9 activity assay

We purchased Caspase-3 Assay Kit (Colorimetric) (ab39401), Caspase-8 Assay Kit (Colorimetric) (ab39700), and Caspase 9 Assay Kit (Colorimetric) (ab65608) from abcam. As per the manufacturer's instructions, the activity of caspase-3, 8, and 9 was measured using a colorimetric assay kit (ab39401, ab39700, ab65608; abcam Boston, USA). 200 μg of cell lysate from treated MOLT-4 cells with nanocomposites of $ZnO + TiO_2$-Chitosan-Amygdalin. Three independent cell cultures were used for each assay. Microplate readers BioTek SynergyMx were used to measuring the absorbance at 405 nm. This formula was used to calculate caspase activity in arbitrary units: absorbance of (sample*control)/control.

2.12. Statistical analysis

SPSS 20.0 was used to conduct the statistical analyses (SPSS Inc., USA). The values are expressed in mean + SD, and the statistical comparison methods were Student's t-test and one-way analysis of variance (ANOVA), with a Tukey's test conducted for additional validation. The value $p < 0.05$ was considered statistically significant.

3. Results

3.1. Physicochemical characterization of ZnO-TiO$_2$-Chitosan-Amygdalin nanocomposites

ZnO-TiO$_2$-Chitosan-Amygdalin nanocomposites containing ZnO-TiO$_2$-Chitosan-Amygdalin were analyzed using FT-IR to determine their various functional groups. The FTIR spectrum of ZnO-TiO$_2$-Chitosan-Amygdalin nanocomposites is exhibit in Fig. 1a. Based on the results of this study, we determined that ZnO, TiO$_2$, chitosan, and Amygdalin are the functional groups for the Nanocomposites. On the chitosan peaks, the broad peaks at 3786 cm^{-1}, 3418 cm^{-1}, and 1632 cm^{-1}, which have —OH and —NH peaks with hydrogen bonds, indicate amide I groups (C—O stretching and N—H deformation). As a result, the peak at 1383 cm^{-1} corresponds to the stretching vibration of C—O—C in the glucose circle, whereas the peak at 1076 cm^{-1} and 1019 cm^{-1} corresponds to COO— a group in the carboxylic acid salt (Karthikeyan et al., 2021). However, the Amygdalin characteristics peaks: The asymmetric and symmetric peaks detected at 2925 cm^{-1} and 2862 cm^{-1}, due to the —C—H(CH$_2$) group, alkane stretching peaks found to 2426 cm^{-1}, C—O stretching peak for 1144 cm^{-1} and —HC=CH out of plane bending peak at 911 cm^{-1} respectively (Yang et al., 2021). The metal–oxygen stretching vibration like Zn—Ti—O is identified at 724, 672, and 547 cm^{-1} (Priyanka et al., 2021). The FTIR spectrum results confirmed that ZnO-TiO$_2$-Chitosan-Amygdalin nanocomposites that chitosan and productively interacted with chitosan and Amygdalin in the ZnO and TiO$_2$ of the ZnO-TiO$_2$-Chitosan-Amygdalin nanocomposites and these exchanges are due to the electrostatic interaction between ZnO-TiO$_2$-Chitosan-Amygdalin nanocomposites surface matrix.

The photoluminescence spectrum of ZnO-TiO$_2$-Chitosan-Amygdalin nanocomposites with an excitation wavelength of 325 nm is shown in Fig. 1b. As expected, peaks of emission were observed at 377 nm, 394 nm, 418 nm, 442 nm, 457 nm, 473 nm, and 509 nm in the ZnO-TiO$_2$-Chitosan-Amygdalin nanocomposites sample. As a result of the radiation recombination of the free exciton–exciton collision process (Lequn et al., 2021), UV emissions were observed at 377 nm and 394 nm. This is due to an electron transition from the zinc interstitials (Zn$_i$) surface to the top level of the valence band at 418 nm (Karthikeyan et al., 2021). During the blue emission bands observed at 442 nm, 457 nm, and 473 nm, the Zn vacancies (V$_{Zn}$) are recorded (Karthikeyan et al., 2021). To study the oxygen vacancies (O$_v$) associated with green emission, a 509 nm wavelength was selected (Karthikeyan et al., 2021).

Functional groups in zinc oxide nanocomposites are indicated by the peaks. As a result, 3786 cm^{-1}, 3418 cm^{-1}, and 1632 cm^{-1} are determined as absorption peaks in the samples. The absorption peak at 614 cm-1 is associated with metal–oxygen stretching vibrations (ZnO-TiO$_2$-Chitosan-Amygdalin). At 1109 cm-1, a stretch vibration of either the C-N or C-O bonds of the primary alcohol is responsible for the peak. Molecular vibration modes of aromatic nitro compounds and alkyl are responsible for the peak at 1650 cm-1. Stretching vibrations of hydroxyl compounds are responsible for peaks at 2855 cm-1 and 3443 cm-1. An FTIR spectrum of ZnO-TiO$_2$-Chitosan-Amygdalin nanocomposites is shown in Fig. 1b. It is possible to observe the vibrations of individual atoms or groups of atoms using FTIR analysis. The ZnO-TiO$_2$-Chitosan-Amygdalin bonds were found to be prevalent in all samples tested, including the commercial sample, which
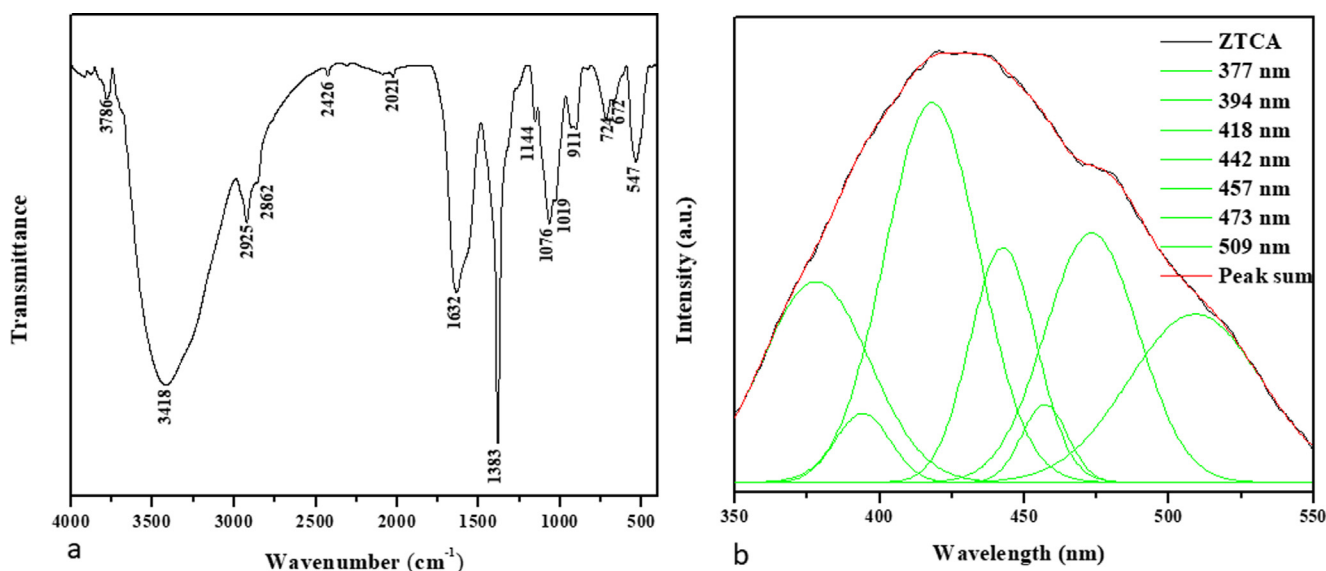
Fig. 1 **Spectral analysis of CuO-TiO$_2$-Chitosan-Berbamine nanocomposites.** FTIR Transmittance vs wavenumber chart of ZnO-TiO$_2$-Chitosan-Amygdalin nanocomposites derived from infrared analysis (a). Photoluminescence spectra for ZnO-TiO$_2$-Chitosan-Amygdalin nanocomposites at room temperature (b).

showed similar behavior. Fig. 1b illustrates the effect of adding ZnO-TiO$_2$-Chitosan-Amygdalin nanocomposites to ZnO-TiO$_2$-Chitosan-Amygdalin nanocomposites, which shows a distinct band at approximately 473 nm which is centered on the graph of the photoluminescence spectrum. Additionally, there is a reduction of absorption when ZnO-TiO$_2$-Chitosan-Amygdalin nanocomposites contain ZnO-TiO$_2$-Chitosan-Amygdalin.

3.2. Transmission electron microscopy (TEM) and scanning electron microscopy (SEM and EDS)

Structural analysis of ZnO-TiO$_2$-Chitosan-Amygdalin nanocomposites is shown in Fig. 2a and b. The surface topography and the Chemical composition of the ZnO-TiO$_2$-Chitosan-Amygdalin nanocomposites were employed by FESEM/TEM/EDAX spectrum, and they are shown in Figs. 2 (a–b) and 3(a–d). FESEM and TEM images indicate that the ZnO-TiO$_2$-Chitosan- Amygdalin nanocomposites exhibit a nano rod-like structure. The results (TEM image 3c) show that the nanorod formation edge (Metal oxide is encapsulated with biopolymer chitosan and Phyto-compounds Amygdalin observed in nanorod top). In accordance with the XRD results, the average particle size was found to be ~65 ± 5 nm. Fig. 3d shows that the TiO$_2$ Amygdalin and chitosan nanomaterial exhibit ZnO Wurtzite hexagonal crystal structure in the selected area of electron diffraction pattern (SAED). In Fig. 4c, the EDAX spectrum for ZnO-TiO$_2$-Chitosan-Amygdalin is displayed. The atomic percentages of the ZnO-TiO$_2$-Chitosan-Amygdalin nanocomposites were: 20.33 % (C), 15.23 % (N), 14.80 % (Zn), 4.89 % (Ti), and 44.72% (O).
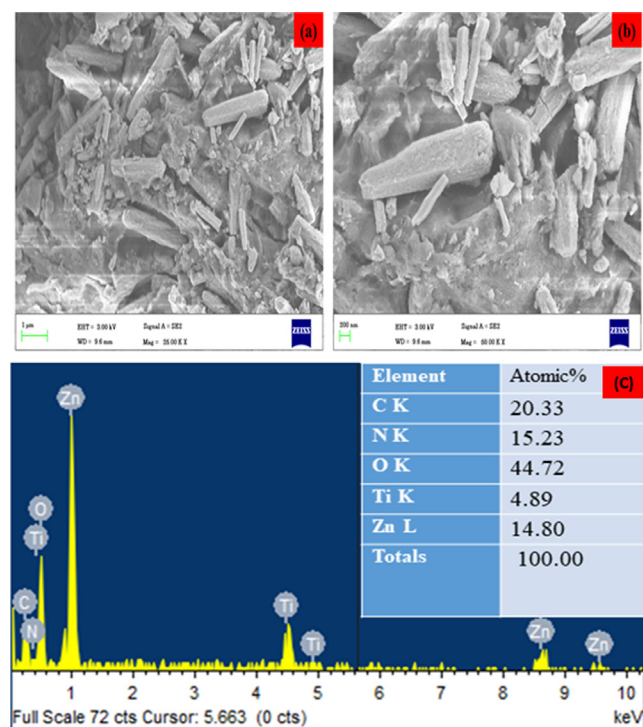
At the magnification used, structures appeared more isolated and clustered as they were homogenous and well dispersed. By incorporating particle dispersion into our DLS calculation (Fig. 3b), we get a larger particle size as a result. ZnO-TiO$_2$-Chitosan-Amygdalin nanocomposites EDAX result is shown in Fig. 2c. Based on stoichiometric calculations, the weight percentages of carbon, nitrogen, and oxygen present in the samples should be 7.10%, 52.60%, 2.06%, and 38.25%, respectively. As determined by the Zn, C, N, and O percentages measured in the samples, ZnO-TiO$_2$-Chitosan-Amygdalin nanocomposites are chemically similar to these amounts (d).

3.3. XRD and DLS

X-ray diffraction patterns of ZnO-TiO$_2$-Chitosan-Amygdalin nanocomposites are shown in Fig. 4a. XRD patterns of ZnO-TiO$_2$-Chitosan-Amygdalin nanocomposites, ZnO appear the predominant face observed at angles (2θ) 31.74°, 34.41°, 36.25°, 47.45°, 56.54°, 62.90°, 66.53°, 67.95°, 69.24° corresponding hkl values are (1 0 0), (0 0 2), (1 0 1), (1 0 2), (1 1 0), (1 0 3), (2 0 0), (1 1 2), (2 0 1), (0 0 4), and (2 0 2) for ZnO (wurtzite hexagonal) phase formation, which closely matched with JCPDS card No. 36-1451. To observe TiO$_2$ peaks angle 2θ at 24.35°, 29.59°, 29.96°, and 44.125°, 48.36°, which revealed that the anatase TiO$_2$ phase (JCPDS card No: 21-1272). However, the typically non-crystalline chitosan are peaked, observed at 10.52° and 19.62°. Moreover, Amygdalin diffraction peaks were found to be 15.84° and 16.20°. According to the results, the ZnO-TiO$_2$-chitosan-Amygdalin phase's formation is the result of steric effects, as well as hydrogen bonds between the ZnO-TiO$_2$-chitosan-Amygdalin molecules. Using the Debye-Scherrer formula, the ZnO-TiO$_2$-Chitosan-Amygdalin matrix had an average crystallite size of 63 nm (Ocakoglu et al., 2015).

Dynamic Light Scattering (DLS) spectrum of synthesized ZnO-TiO$_2$-Chitosan- Amygdalin nanocomposites were ~139.40 nm. In addition, DLS particle size was increased compared to the XRD and TEM results because the nanocomposites were surrounded by a water medium; this is known as hydrodynamic size (Fig. 4b).

3.4. ZnO-TiO$_2$-Chitosan-Amygdalin nanocomposites cause cytotoxicity in MOLT-4 cells

Study on cytotoxicity of ZnO-TiO$_2$-Chitosan-Amygdalin nanocomposites with the following concentrations: 2.5, 5, 7.5, 10, 12.5, and 15 µg/ml. Upon administration of ZnO-TiO$_2$-Chitosan-Amygdalin nanocomposites to MOLT-4 cells, a dose-dependent reduction in cell viability is observed with an IC$_{50}$ concentration of 10.34 µg/ml. Treatment with 7.5 and 10 µg/ ml resulted in above 40% of cell death. So, we utilized both 7.5 µg and 10 µg ZnO-TiO$_2$-Chitosan-Amygdalin nanocomposites in further cellular studies(Fig. 5).

Element	Atomic%
C K	20.33
N K	15.23
O K	44.72
Ti K	4.89
Zn L	14.80
Totals	100.00

Full Scale 72 cts Cursor: 5.663 (0 cts)

Fig. 2 SEM micrographics of the ZnO-TiO$_2$-Chitosan-Amygdalin nanocomposites: Lower magnification of surface (a), Lower magnification of surface (b), elements, weight %, and atomic % of the composition obtained by EDX (c).
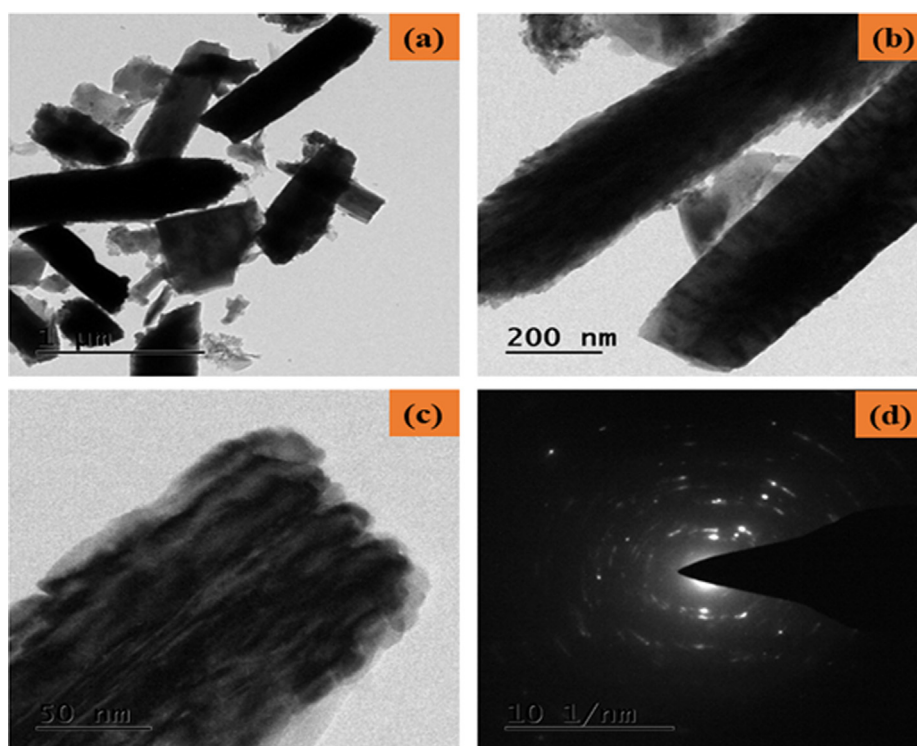
Fig. 3　TEM micrographics of the ZnO-TiO$_2$-Chitosan-Amygdalin nanocomposites: Lower and Higher magnification TEM image (a-c) and SAED pattern of ZnO-TiO$_2$-Chitosan-Amygdalin nanocomposites (d).
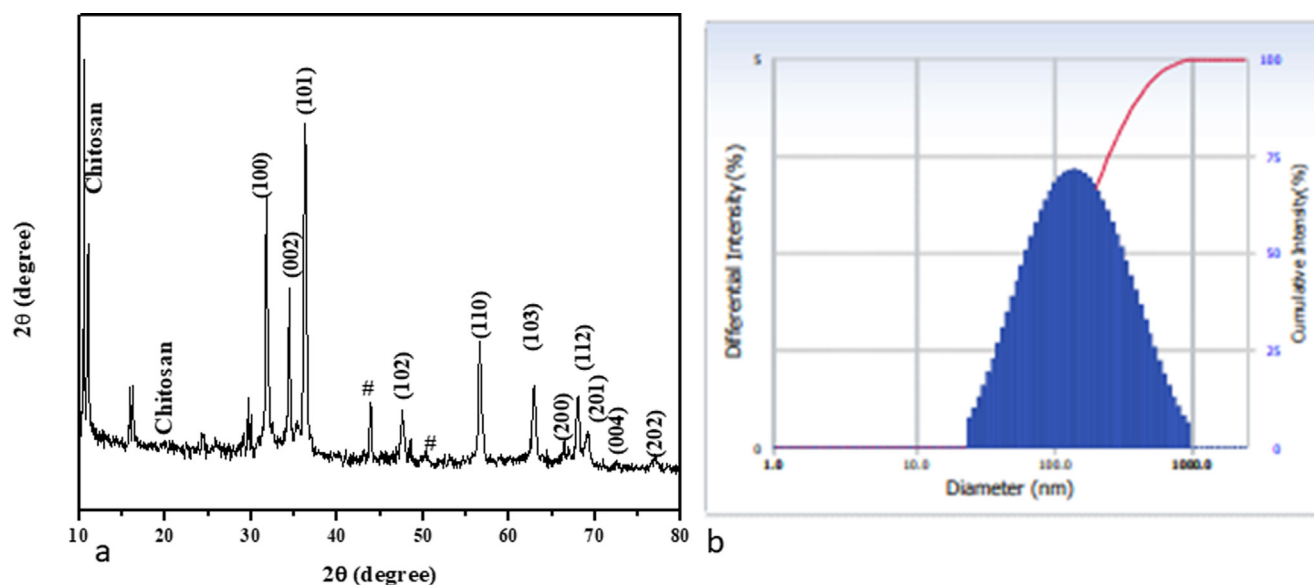
Fig. 4 XRD Pattern of ZnO-TiO$_2$-Chitosan-Amygdalin nanocomposites (a). Number-weighted particle size distribution, obtained by DLS (b).

3.5. The MOLT-4 cell line is apoptotic in response to ZnO-TiO$_2$-Chitosan-Amygdalin nanocomposites

ZnO-TiO$_2$-Chitosan-Amygdalin nanocomposites and doxorubicin treated AO/EtBr stained MOLT-4 cells. Green fluorescence is greater in control cells with intact nuclei, while green fluorescence is greater in 7.5 µg/ml ZnO-TiO$_2$-Chitosan-Amygdalin nanocomposites-treated cells, indicating early apoptotic cells. We observed an increase in the proportion of orange-fluorescent late apoptotic cells in cells treated with 10 µg/ml of ZnO-TiO$_2$-Chitosan-Amygdalin nanocomposites (Fig. 6). The control cells showed green fluorescence that indicates living cells without apoptosis. The ZnO-TiO$_2$-Chitosan-Amygdalin nanocomposites tested cells showed yellow and orange fluorescence, which indicates early and late apoptotic cell death, respectively with condensed or fragmented nuclei
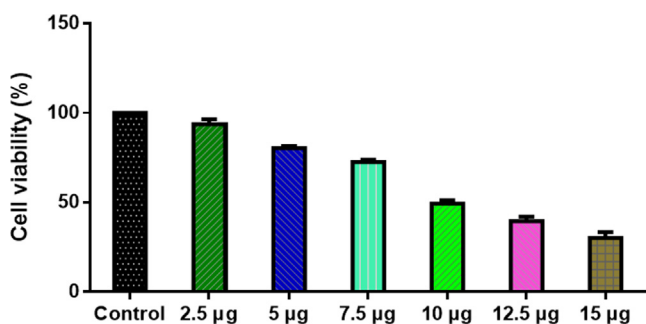
Fig. 5 ZnO-TiO₂-Chitosan-Amygdalin nanocomposites cause cytotoxicity in MOLT-4 cells. MOLT-4 cell lines were treated with different concentrations (2.5 – 1.5 μg/ml) of ZnO-TiO₂-Chitosan-Amygdalin nanocomposites for 24 h. The cells were subjected to an MTT assay and the values were depicted as ± SD of three individual experiments.

3.6. ZnO-TiO₂-Chitosan-Amygdalin nanocomposites induce ROS generation in MOLT-4 cell line

A DCFH-DA staining of MOLT-4 cells was used to evaluate the reactive oxygen species generated by ZnO-TiO₂-Chitosan-Amygdalin nanocomposites. In the control, cells show no fluorescent, 7.5 μg/ml of ZnO-TiO₂-Chitosan-Amygdalin nanocomposites treated cells fewer fluorescent were observed while the 10 μg/m of ZnO-TiO₂-Chitosan-Amygdalin nanocomposites treated samples showed more fluorescent cells (Fig. 7). Control cells showed a low intensity of green fluorescence that indicates poor ROS generation. The ZnO-TiO₂-Chitosan-Amygdalin nanocomposites (7.5 and 10 μg/ml) treated cells showed a bright green fluorescence, which confirms the increased ROS production in MOLT-4 cells (Fig. 7).

3.7. The mitochondrial membrane permeability in MOLT-4 cells is impaired by ZnO-TiO₂-Chitosan-Amygdalin nanocomposites

Apoptosis was believed to be triggered by an increase in mitochondrial membrane permeability. So we performed Rhodamine 123 staining on treated and untreated cells to

and necrotic cells. Apoptosis was detected by AO/EtBr staining, with an increase of 25–40% apoptosis by 24 h at concentrations of 10 μg/ml when compared to 7.5 μg/ml (Fig. 6).
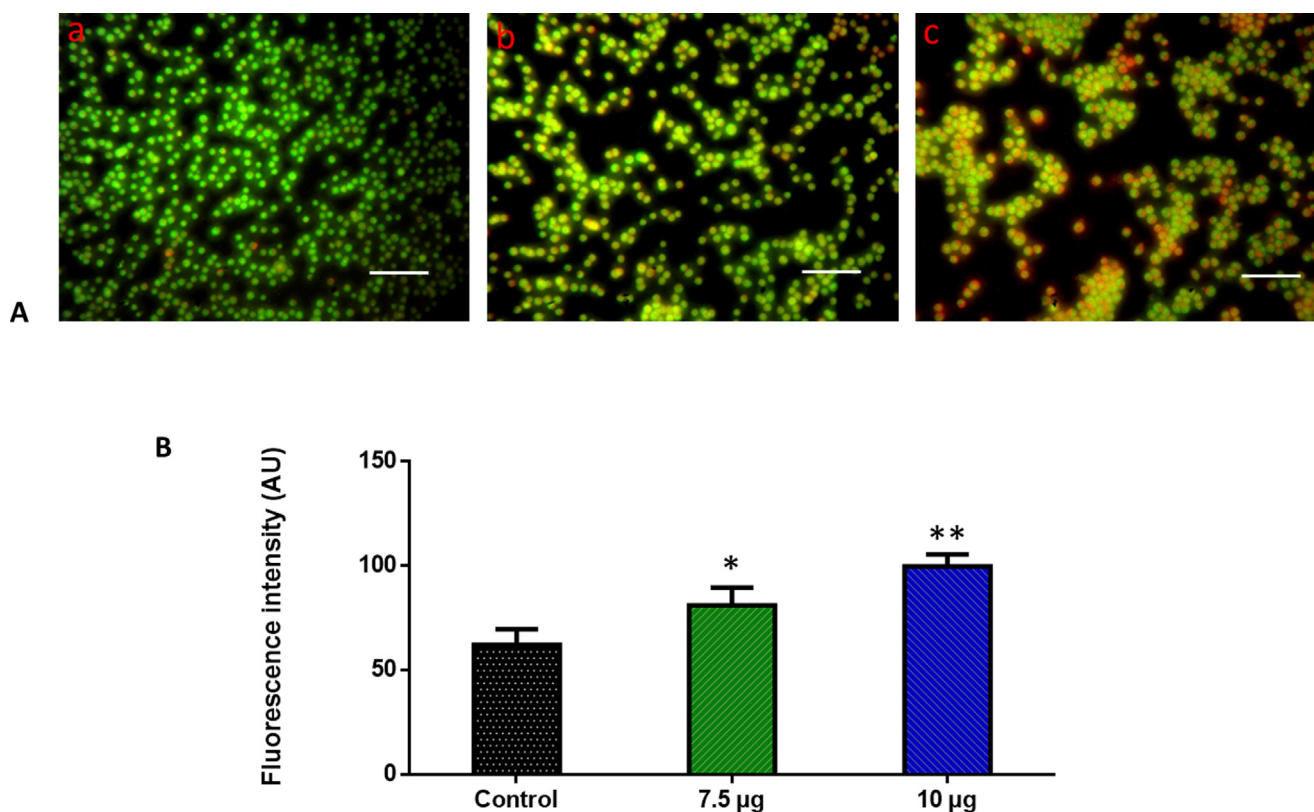
Fig. 6 Effect of ZnO-TiO₂-Chitosan-Amygdalin nanocomposites on the apoptotic cell death in the blood cancer MOLT-4 cells for 24 h. Acridine orange and ethidium bromide (1:1), was used to stain the cells, then analyzed by fluorescence microscopy (Labomed, USA). The control cells showed green fluorescence that indicates living cells without apoptosis. The ZnO-TiO₂-Chitosan-Amygdalin nanocomposites tested cells showed yellow and orange fluorescence, which indicates early and late apoptotic cell death, respectively with condensed or fragmented nuclei and necrotic cells. Panel A; Control (a) (untreated cells), ZnO-TiO₂-Chitosan-Amygdalin nanocomposites-treated cells; 7.5 μg/ml concentration (b) and 10 μg/ml concentration (c). Panel B; Arbitrary Units (a.u.) of fluorescent Intensity from the control and treated cells incubated at 37 °C were measured by a fluorescence microplate reader. *p < 0.05 compared to the "Control" group and **p < 0.005 compared to the "Control" group. Scale Bar = 25 μm.
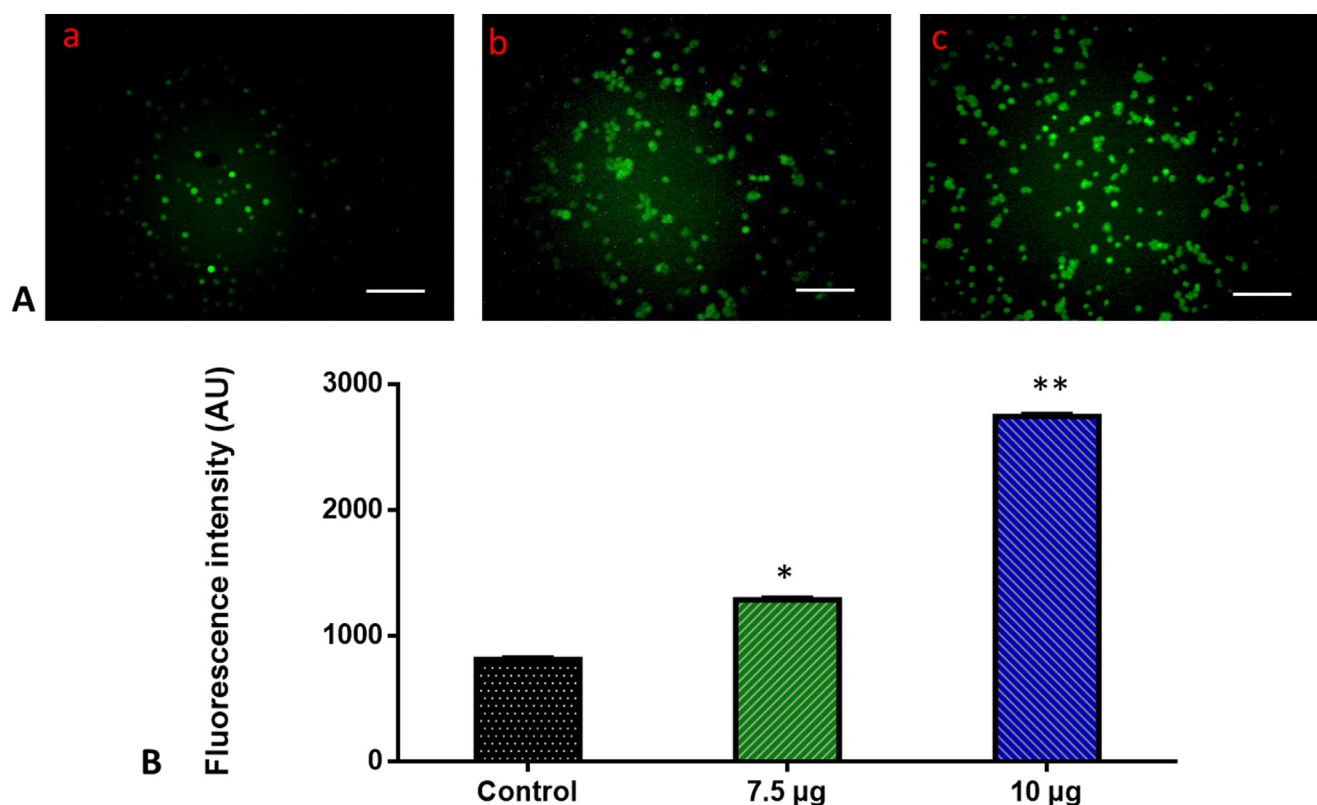
Fig. 7 **Effect of ZnO-TiO$_2$-Chitosan-Amygdalin nanocomposites on the intracellular ROS generation in the blood cancer MOLT-4 cells.**
The MOLT-4 cell line is subjected to oxidative stress induced by ZnO-TiO$_2$-Chitosan-Amygdalin nanocomposites were staining with DCFH-DA. Then the digital images were captured by a Fluorescence microscope (Labomed, USA). Control cells showed a dull green fluorescence that indicates poor ROS generation. The ZnO-TiO$_2$-Chitosan-Amygdalin nanocomposites (7.5 and 10 μg/ml) treated cells showed a bright green fluorescence, which confirms the increased ROS production in MOLT-4 cells. Panel A; Control (a) (untreated cells), ZnO-TiO$_2$-Chitosan-Amygdalin nanocomposites-treated cells; 7.5 μg/ml concentration (b) and 10 μg/ml concentration (c). Panel B; Arbitrary Units (a.u.) of fluorescent Intensity from the control and treated cells incubated at 37 °C were measured by a fluorescence microplate reader. *p < 0.05 compared to the "Control" group and **p < 0.005 compared to the "Control" group. Scale Bar = 25 μm.

examine the mitochondrial membrane permeability. 7.5 μg/ml of ZnO-TiO$_2$-Chitosan-Amygdalin nanocomposites-treated cells have fewer fluorescent cells in comparison with 10 μg/ml of ZnO-TiO$_2$-Chitosan-Amygdalin nanocomposites cells and control cells showed greater fluorescence (Fig. 8). Control cells showed a bright fluorescence that indicates a higher MMP level. The ZnO-TiO$_2$-Chitosan-Amygdalin nanocomposites (7.5 and 10 μg/ml) treated cells showed a dull or decreased green fluorescence, which indicates the reduced MMP level in MOLT-4 cells (Fig. 8).

3.8. Induction of apoptosis in MOLT-4 cells was by ZnO-TiO$_2$-Chitosan-Amygdalin nanocomposites

In untreated Molt-4 cells, apoptotic nuclei were observed at varying times 24 h after treatment with ZnO-TiO$_2$-Chitosan-Amygdalin nanoparticles. Nuclei that undergo apoptosis increase in a time-dependent manner with clear condensation fragmentation. Which was confirmed by measuring the activate the pro-apoptotic proteins, caspases. NPs of ZnO-TiO$_2$-Chitosan-Amygdalin were studied in 24 hr experiments and evaluated for caspase activation. As determined by colorimetric assay, ZnO-TiO$_2$-Chitosan-Amygdalin NPs significantly increased the caspase-3, 8, and 9 activity compared to untreated cells (p < 0.05). A caspase-3, 8, and 9 activation assay demonstrated that ZnO-TiO$_2$-Chitosan-Amygdalin NPs induced these activities in Molt-4 cells. Induction of apoptosis by ZnO-TiO$_2$-Chitosan-Amygdalin NPs is accompanied by caspase activation (Fig. 9).

4. Discussion

The disorders of hematopoietic stem cells are lymphoblastic leukemia (ALL) and lymphoblastic lymphoma (LBL). Children with acute leukemia make up 30 percent of all childhood cancers (Marison et al., 2021). Malignant tumors with unique biological features, such as human ALL, are extremely aggressive and difficult to diagnose. According to the WHO classification system (Kaseb et al., 2022), these diseases are classified as precursor lymphoid neoplasms. The disease's surgical resection, chemotherapy, and radiotherapy are all unsatisfactory. It is necessary to develop novel adjuvant medicines, prospective anticancer drugs, and human ALL that can be treated using molecularly targeted therapies based on a thorough investigation of biological characteristics and metastatic mechanisms.
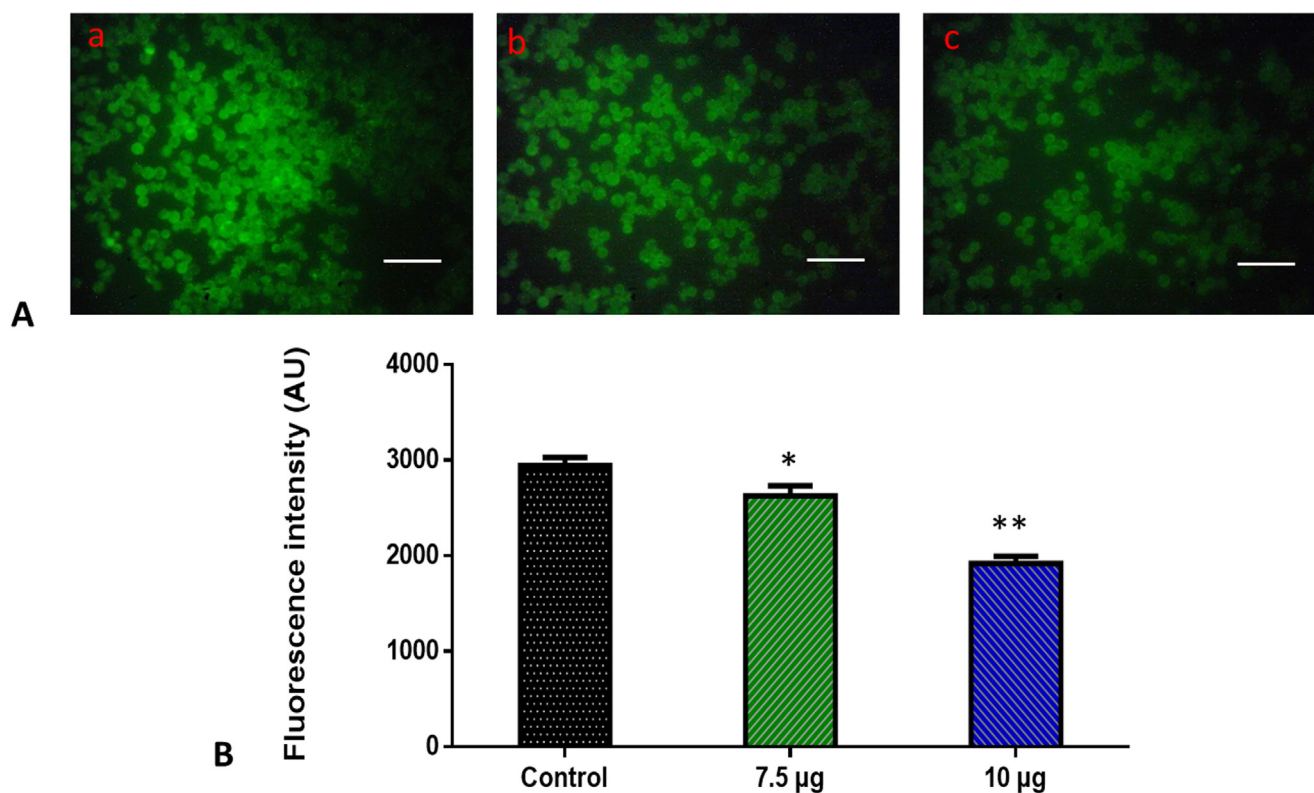
Fig. 8   Effects of ZnO-TiO$_2$-Chitosan-Amygdalin nanocomposites on the mitochondrial membrane potential in the blood cancer MOLT-4 cells. MOLT-4 cells with ZnO-TiO$_2$-Chitosan-Amygdalin nanocomposites present have a decreased mitochondrial membrane permeability. Rhodamine 123 was used to stain the cells. The fluorescent images were captured by a Fluorescence microscope (Labomed, USA). Control cells showed a bright fluorescence that indicates a higher MMP level. The ZnO-TiO$_2$-Chitosan-Amygdalin nanocomposites (7.5 and 10 µg/ml) treated cells showed a dull or decreased green fluorescence, which indicates the reduced MMP level in MOLT-4 cells. Panel A; Control (a) (untreated cells), ZnO-TiO$_2$-Chitosan-Amygdalin nanocomposites-treated cells; 7.5 µg/ml concentration (b) and 10 µg/ml concentration (c). Panel B; Arbitrary Units (a.u.) of fluorescent Intensity from the control and treated cells incubated at 37 °C were measured by a fluorescence microplate reader. *p < 0.05 compared to the "Control" group and **p < 0.005 compared to the "Control" group. Scale Bar = 25 µm.

Nanomedicine seeks to solve problems associated with biological molecules that exist, are formed, and perform most of their functions at the nanoscale (Vinhas et al., 2017). Nanotechnology has improved the in vivo efficacy of anti-cancer therapies by regulating the release of their drugs. Nanocomposites are recognized for their inherent anticancer properties due to their biological properties (Kemp and Kwon, 2021). Molecularly synthesized nanocomposite materials have anticancer properties due either to intrinsic characteristics, such as antioxidant activity, or excessive heat generated by infrared radiation or magnetic fields under external stimulation. Nanocomposites can potentially interact with blood vessels or stroma surrounding tumors, preventing them from growing (Samir et al., 2015).

The functional groups of produced ZnO-TiO$_2$-Chitosan-Amygdalin NPs were investigated and determined using FTIR (Fig. 1a). In FTIR spectrum analysis, a broad absorption band was observed in 547–3786 cm^{-1} that features ZnO-TiO$_2$-Chitosan-Amygdalin stretching vibration. In earlier studies of ZnO-TiO$_2$-Chitosan-Amygdalin nanoparticles, FTIR with a band at 3418 cm^{-1} was also observed at maximum. The absorption peak was detected at 377, 394, 418,442,457,473, and 509 nm, indicating that ZnO-TiO$_2$-Chitosan-Amygdalin

absorption has an intrinsic band-gap in Photoluminescence spectra (Fig. 1b). Previous studies also found a similar finding for the absorption band that represents ZnO-TiO$_2$-Chitosan-Amygdalin NPs, with the range of absorption band being 355–380 nm. SEM analysis of the nanoparticles revealed that they were clustered by shape, closely related in size, and distributed fairly (Fig. 2a and b). EDS analysis was beneficial in controlling the stoichiometry and purity of nanocomposites. EDS pattern that indicates the presence of Zn, C, N, and O elements, and no impurity peaks are visible (Fig. 2c and d). The appropriate Kα line from the X-ray spectra was used to calculate the dispersal of each element (C, O, N, and Zn). The EDS mapping images show that the samples are mostly homogeneous, with some localized aggregation of nanocomposites developing as the ZnO-TiO$_2$-Chitosan-Amygdalin percentage rises. The residual peaks are indexed to ZnO-TiO$_2$-Chitosan-Amygdalin's hexagonal structure, which matches the standard data. The XRD data showed that after calcination, the precursors had completely transformed into ZnO-TiO$_2$-Chitosan-Amygdalin crystals. The well-ordered crystalline samples are shown by the strong and sharp peaks (Fig. 4a).

These results are following other research that has found ZnO-TiO$_2$-Chitosan-Amygdalin NPs drastically enhance cyto-
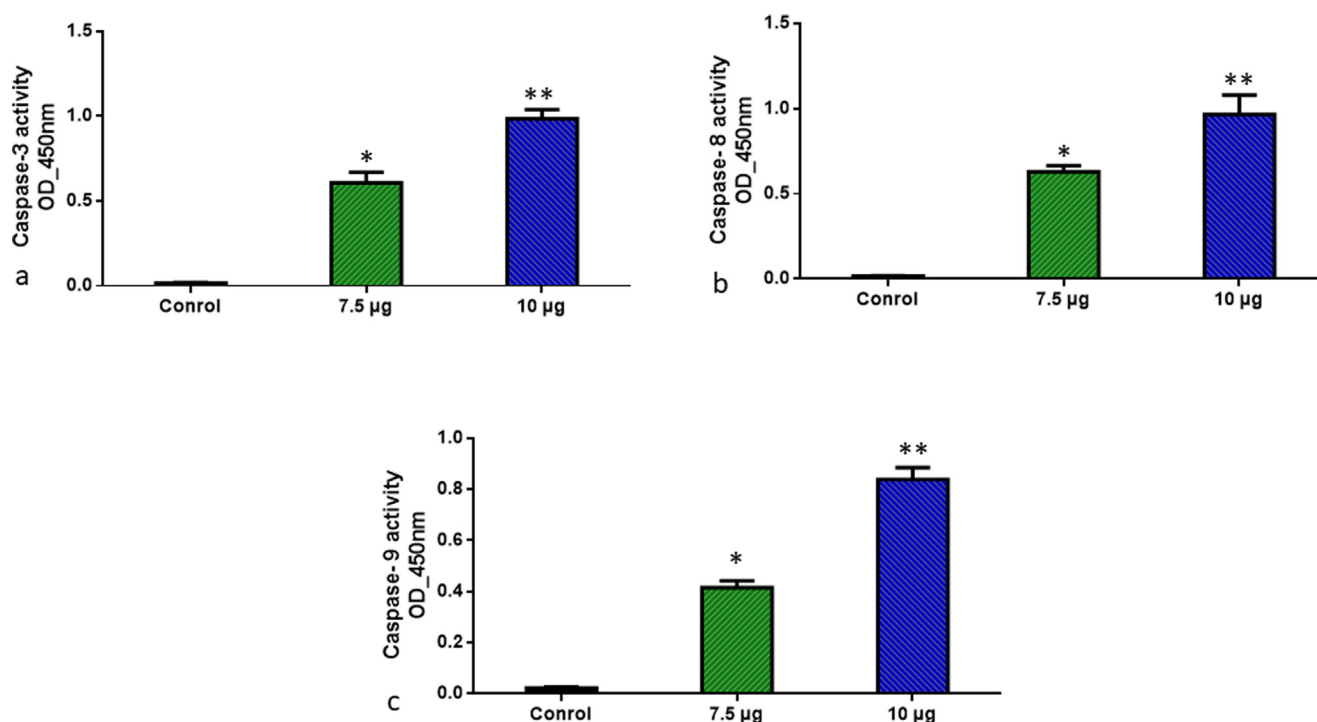
Fig. 9   ZnO-TiO₂-Chitosan-Amygdalin nanocomposites induced pro-apoptotic response Caspase-3, 8, and 9 in the MOLT-4 cell line. The colorimetric quantification of active Caspase-3, 8, and 9 in MOLT-4 cell line after 24-h treatment of 7.5 and 10 µg/ml concentration of ZnO-TiO₂-Chitosan-Amygdalin nanocomposites. The data were presented as activity of caspase –3, 8, and 9 enzymes and mean ± SEM. n = 6, *p < 0.05 compared to the "Control" group and **p < 0.005 compared to the "Control" group.

toxicity and apoptotic cell death in Molt-4 cancer cells (Figs. 5 and 6), while normal cells are essentially unaffected. In-vivo characterization of magnetic compounds coupled to nanoparticles (NPs) could provide novel characteristics for the nanocomposites that enhance site-directed cancer chemotherapy. Previous studies have demonstrated the ability to synthesize ZnFe2O4@Ag nanocomposites using *Scenedesmus obliquus* extract, and to characterize its antiproliferative capacity against breast cancer cells (MCF-7) via caspase-3, 8, and p53-mediated apoptosis. ZnFe2O4@Ag exhibits significant cytotoxicity against the MCF-7 breast cancer cell line (IC$_{50}$ = 111 µg/mL) when compared to the HEK-293 (normal) cell line (IC$_{50}$ = 372 µg/mL) (Jodati et al., 2022). The study synthesized and characterized TiFe2O4@Ag NPs silver nanocomposites using *Spirulina platensis* and showed that it was significantly more cytotoxic toward AGS gastric cancer cells (IC$_{50}$ = 69.6 µg/mL) than normal HEK293 cells (IC$_{50}$ = 130 µg/mL), which showed apoptosis and higher levels of Bax, p53, and Bcl-2 Gene expression (Tabassi et al., 2021). ZnO-TiO₂-Chitosan-Amygdalin nanoparticles were found to be cytotoxic to human umbilical vein endothelial cells (HUVECs), but not to normal human astrocytes (Kandile et al., 2002; Schirinzi et al., 2017; Yan et al., 2021). Zn-based NPs have been shown to selectively (or preferentially) trigger apoptosis in cancer cells rather than normal cells on numerous occasions and exhibit potent antimicrobial activity also (Bui et al., 2017). Several kinds of literature have confirmed the link between increased intracellular ROS and cytotoxicity of nano-sized compounds. In both normal and stressful circumstances, ROS can execute a variety of roles such as activator of cell growth and development in normal conditions but under

stressful situations, it may lead to not only pathological abnormalities but also cell death (Pujalté et al., 2011; Suresh et al., 2018; Ali et al., 2018). In our study, the apoptotic process is triggered by high amounts of intracellular ROS by the action of ZnO-TiO₂-Chitosan-Amygdalin NPs (Fig. 7). Due to the weakening of responsive genes, it is critical to keep an eye on the depolarized membrane of mitochondria (Fig. 8).

When the mitochondrial membrane is disturbed, the suppressive genes of the caspase family, are activated limiting the production of cancer cell responsive genes. Intracellular leakage materials were lost after Rhodamine 123 was infused into the mitochondrial membrane, and their color changed from red to green, indicating apoptosis (Fig. 8). Our results showed that activation of apoptotic cell death via Caspases dependent mitochondrial-mediated pathway when treated with 7.5 and 10 µg/ml ZnO-TiO₂-Chitosan-Amygdalin nanocomposites when compared to control MOLT-4 cells (Fig. 9).

Apoptosis can be triggered by several genes, such as Bcl-2 and caspases (McIlwain et al., 2015). Our findings show that Caspase-3, 8, and 9 do not cause apoptosis, however, it has been shown that it reduces cellular resistance to apoptotic stimuli, thus triggering apoptosis. Caspases, enzymes that degrade aspartic acid, are primarily involved in apoptosis. Apoptosis involves caspase-dependent and caspase-independent processes. Caspase 3, 8, and 9 were activated by ZnO-TiO₂-Chitosan-Amygdalin nanoparticles as shown in the present study. Accordingly, ZnO-TiO₂-Chitosan-Amygdalin NPs produce both caspase-dependent and caspase-independent apoptosis in MOLT-4 cells. Using the human leukemia cell line MOLT-4, we have shown the efficacy of CuNPs derived from the *C. Sinensis* (Mendhulkar Vijay and

Yadav, 2017) and CoII-quinalizarin, an anthracycline-based anticancer agent analog (Sayantani Mukherjee et al., 2018). Studies have shown that ZnO-C nanocrystals had significantly lower cytotoxicity than synthetic ZnO-C nanocrystals against HEp2 cells, suggesting they have greater therapeutic potential (Dananjaya et al., 2018).

In addition to demonstrating ZnO-TiO$_2$-Chitosan-Amygdalin nanocomposite's anti-cancer efficacy in its particular proof-of-concept study found that ZnO-TiO$_2$-Chitosan-Amygdalin nanocomposites had increased potency and specificity on the human MOLT-4 cell line when compared to ZnO-TiO$_2$-Chitosan-Amygdalin nanocomposites. Our findings show that polymer conjugation can boost ZnO-TiO$_2$-Chitosan-Amygdalin nanocomposite's inhibitory activity by promoting apoptosis, lowering cellular growth, and perhaps chemoresistance circumvention.

5. Conclusion

In our study, ZnO-TiO$_2$-Chitosan-Amygdalin nanocomposites were synthesized and studied using SEM, TEM, FTIR, and XRD measurements. The synthesized ZnO-TiO$_2$-Chitosan-Amygdalin nanocomposites inhibited leukemia cell proliferation in a dose-dependent manner. ZnO-TiO$_2$-Chitosan-Amygdalin nanocomposites showed anticancer activity by triggering apoptosis through the mitochondrial pathway. In the treated cells with ZnO-TiO$_2$-Chitosan-Amygdalin nanocomposites, apoptosis was significantly increased with increases in caspase 3, 8, and 9 activities (p < 0.001), as well as an increase in the number of early and late apoptotic cells (p < 0.001). Nanocomposites of ZnO-TiO$_2$-Chitosan-Amygdalin characterized by cytotoxicity resulted in significantly reduced polarized mitochondrial membranes as well as increased depolarized mitochondrial membranes. Results showed that ZnO-TiO$_2$-Chitosan-Amygdalin nanocomposites promoted cytotoxicity, caspase 3, 8, and 9 activity, depolarized mitochondrial membrane potential, and ROS production as well as decreased cellular proliferation, ultimately supporting their high uptake and anticancer properties. In MOLT-4 human leukemia cells, we have demonstrated mechanistically that ZnO-TiO$_2$-Chitosan-Amygdalin nanocomposites activate the intrinsic apoptotic pathway. Further studies are to be conducted to determine whether ZnO-TiO$_2$-Chitosan-Amygdalin nanocomposites have cytotoxic properties against cancer cells. The synthesized ZnO-TiO$_2$-Chitosan-Amygdalin nanocomposites may prove to be a real blessing for cancer patients since they show great promise for providing a more effective, safer, cheaper, and most importantly targeted cancer treatment.

Availability of data and material

The data which support the findings of this research are available from the corresponding author.

Acknowledgment

Declaration of Competing Interest

The authors declare that they have no known competing financial interests or personal relationships that could have appeared to influence the work reported in this paper.

References

Aberuyi, N., Rahgozar, S., Ghodousi, E.S., Ghaedi, K., 2020. Drug Resistance Biomarkers and Their Clinical Applications in Childhood Acute Lymphoblastic Leukemia. Front. Oncol. 17, 1496. https://doi.org/10.3389/fonc.2019.01496. PMID: 32010613; PMCID: PMC6978753.

Ali, A., Phull, A.-R., Zia, M., 2018. Elemental zinc to zinc nanoparticles: is ZnO NPs crucial for life? Synthesis, toxicological, and environmental concerns. Nanotechnol. Rev. 7, 413–441. https://doi.org/10.1515/ntrev-2018-0067.

Balsat, M., Cacheux, V., Carre, M., Tavernier-Tardy, E., Thomas, X., 2020. Treatment and outcome of Philadelphia chromosome-positive acute lymphoblastic leukemia in adults after relapse. Expert Rev. Anticancer Ther. 20 (10), 879–891. https://doi.org/10.1080/14737140.2020.1832890. Epub 2020 Oct 15 PMID: 33016157.

Bui, V.K.H., Park, D., Lee, Y.C., 2017. Chitosan Combined with ZnO, TiO$_2$ and Ag Nanoparticles for Antimicrobial Wound Healing Applications: A Mini-Review of the Research Trends. Polymers (Basel) 9 (1), 21. https://doi.org/10.3390/polym9010021. PMID: 30970696; PMCID: PMC6432267.

Chang, J.H., Poppe, M.M., Hua, C.-H., Marcus, K.J., Esiashvili, N., 2021. Acute lymphoblastic leukemia. PediatrBlood Cancer 68,. https://doi.org/10.1002/pbc.28371 e28371.

Dai, Q., Zhang, G., Yang, H., Wang, Y., Ye, L., Peng, L., Shi, R., Guo, S., He, J., Jiang, Y., 2021. Clinical features and outcome of pediatric acute lymphoblastic leukemia with low peripheral blood blast cell count at diagnosis. Medicine 100, (4). https://doi.org/10.1097/MD.0000000000024518 e24518.

Dananjaya, S.H.S., Kumar, R.S., Yang, M., Nikapitiya, C., Lee, J., De Zoysa, M., 2018. Synthesis, characterization of ZnO-chitosan nanocomposites and evaluation of its antifungal activity against pathogenic Candida albicans. Int J Biol Macromol. 108, 1281–1288. https://doi.org/10.1016/j.ijbiomac.2017.11.046. Epub 2017 Nov 10 PMID: 29129632.

Inaba, H., Mullighan, C.G., 2020. Pediatric acute lymphoblastic leukemia. Haematologica 105 (11), 2524–2539. https://doi.org/10.3324/haematol.2020.247031. PMID: 33054110; PMCID: PMC7604619.

Inaba, H., Pui, C.H., 2021. Advances in the Diagnosis and Treatment of Pediatric Acute Lymphoblastic Leukemia. J Clin Med. 10 (9), 1926. https://doi.org/10.3390/jcm10091926. PMID: 33946897; PMCID: PMC8124693.

Javed, R., Rais, F., Fatima, H., Haq, I.U., Kaleem, M., Naz, S.S., Ao, Q., 2020. Chitosan encapsulated ZnO nanocomposites: Fabrication, characterization, and functionalization of bio-dental approaches. Mater Sci Eng C Mater Biol Appl. 116,. https://doi.org/10.1016/j.msec.2020.111184. Epub 2020 Jun 11 PMID: 32806262 111184.

Jodati, S., Gorji, S., Sharif, A.P., et al, 2022. A Novel Biosynthesized ZnFe2O4@Ag Nanocomposite: Implications for Cytotoxicity, Gene Expression and Antiproliferative Studies in Breast Cancer Cell Line. J. Clust. Sci. https://doi.org/10.1007/s10876-022-02234-5.

Jung, R., Jacobs, U., Krumbholz, M., Langer, T., Keller, T., De Lorenzo, P., Valsecchi, M.G., van der Velden, V.H., Moericke, A., Stanulla, M., Teigler-Schlegel, A., Panzer-Gruemayer, E.R., van Dongen, J.J., Schrappe, M., den Boer, M.L., Pieters, R., Rascher, W., Metzler, M., 2010. Bimodal distribution of genomic MLL breakpoints in infant acute lymphoblastic leukemia treatment. Leukemia 24 (4), 903–907. https://doi.org/10.1038/leu.2010.14. Epub 2010 Feb 18 PMID: 20164851.

Kandile, N.G., Mohamed, H.M., Nasr, A.S., 2002. Novel hydrazinocurcumin derivative loaded chitosan, ZnO, and au nanoparticles formulations for drug release and cell cytotoxicity. Int. J. Biol. Macromol. 6. https://doi.org/10.1016/j.ijbiomac.2020.05.015. S0141–8130(20)33159-7. Epub ahead of print. PMID: 32387612.

Karthikeyan, C., Tharmalingam, N., Varaprasad, K., Mylonakis, E., Yallapu, M.M., 2021. Biocidal and biocompatible hybrid nanomaterials from biomolecule chitosan, alginate and ZnO. Carbohydr. Polym. 274, 118646.

Kaseb, H., Tariq, M.A., Gupta, G., 2022. Lymphoblastic Lymphoma. 2021 Aug 24. In: StatPearls [Internet]. Treasure Island (FL): StatPearls Publishing; PMID: 30725922.

Kato, M., Manabe, A., 2018. Treatment and biology of pediatric acute lymphoblastic leukemia. Pediatr. Int. 60 (1), 4–12. https://doi.org/10.1111/ped.13457. PMID: 29143423.

Kemp, J.A., Kwon, Y.J., 2021. Cancer nanotechnology: current status and perspectives. Nano Convergence 8, 34. https://doi.org/10.1186/s40580-021-00282-7.

Kustiningsih, I., Ridwan, A., Abriyani, D., Syairazy, M., Kurniawan, T., Barleany, D.R., 2019. Development of Chitosan-TiO$_2$ Nanocomposite for Packaging Film and its Ability to Inactive Staphylococcus Aureus. Orient. J. Chem. 35 (3).

Lequn, L.i., Chujun, Y., Li, W.u., Kai, J., Zhigao, H.u., Ning, X.u., Jian, S., Jiada, W.u., 2021. ZnS Covering of ZnO Nanorods for Enhancing UV Emission from ZnO. J. Phys. Chem. C 125 (25), 13732–13740. https://doi.org/10.1021/acs.jpcc.1c02971.

Marison Jr., S.R., Pati, B., Laferriere, N.R., Woo, R.K., Ha, A., 2021. Unexpected diagnosis of acute lymphoblastic leukemia in a 2-year-old with acute appendicitis - Case report. Int. J. Surg. Case Rep. 84. https://doi.org/10.1016/j.ijscr.2021.106077. Epub 2021 Jun 9. PMID: 34167071; PMCID: PMC8227831.

McIlwain, D.R., Berger, T., Mak, T.W., 2015. Caspase functions in cell death and disease. Cold Spring Harb. Perspect. Biol. 7 (4), a026716. https://doi.org/10.1101/cshperspect.a026716. Erratum for: Cold Spring Harb Perspect Biol. 2013 Apr; 5(4):a008656. PMID: 25833847; PMCID: PMC4382736.

Mendhulkar Vijay, D., Yadav, A., 2017. Anticancer activity of *camellia sinensis* mediated copper nanoparticles against ht-29, mcf-7 and molt-4 human cancer cell lines. Asian J. Pharm. Clin. Res. 10, 82–88. https://doi.org/10.22159/ajpcr.2017.v10i2.15710.

Ocakoglu, K., Mansour, S.A., Yildirimcan, S., Al-Ghamdi, A.A., El-Tantawy, F., Yakuphanoglu, F., 2015. Microwave-assisted hydrothermal synthesis and characterization of ZnO nanorods. Spectrochim. Acta A Mol. Biomol. Spectrosc. 5 (148), 362–368. https://doi.org/10.1016/j.saa.2015.03.106. Epub 2015 Apr 11 PMID: 25913135.

Priyanka, V., Murali, M.K., Rahman, M.A., 2021. Biocidal Properties of Zinc Oxide-Titanium Dioxide-Graphene Oxide Nanocomposites via One-Pot Facile Precipitation Method. BioNanoScience, 1–8.

Pujalté, I., Passagne, I., Brouillaud, B., Tréguer, M., Durand, E., Ohayon-Courtès, C., L'Azou, B., 2011. Cytotoxicity and oxidative stress induced by different metallic nanoparticles on human kidney cells. Part. Fibre Toxicol. 8, 10. https://doi.org/10.1186/1743-8977-8-10.

Samir, A., Elgamal, B.M., Gabr, H., Sabaawy, H.E., 2015. Nanotechnology applications in hematological malignancies (Review). Oncol. Rep. 34, 1097–1105.

Sayantani Mukherjee, C., Chetan Kumar, J., Soumen, S., Piyal, D., Susanta, R., Kumar, H., Majumder, S.D., 2018. Activity of CoII–Quinalizarin: A Novel Analogue of Anthracycline-Based Anti-cancer Agents Targets Human DNA Topoisomerase, Whereas Quinalizarin Itself Acts via Formation of Semiquinone on Acute Lymphoblastic Leukemia MOLT-4 and HCT 116 Cells. ACS Omega 3 (8), 10255–10266. https://doi.org/10.1021/acsomega.8b00706.

Schirinzi, G.F., Pérez-Pomeda, I., Sanchís, J., Rossini, C., Farré, M., Barceló, D., 2017. Cytotoxic effects of commonly used nanomaterials and microplastics on cerebral and epithelial human cells. Environ. Res. 159, 579–587. https://doi.org/10.1016/j.envres.2017.08.043. Epub 2017 Sep 11 PMID: 28898803.

Siegel, R.L., Miller, K.D., Fuchs, H.E., Jemal, A., 2021. Cancer Statistics. CA Cancer J. Clin. 71 (1), 7–33. https://doi.org/10.3322/caac.21654. Epub 2021 Jan 12. Erratum in: CA Cancer J Clin. 2021 Jul;71(4):359. PMID: 33433946.

Subbarayan, S., Marimuthu, S.K., Nachimuthu, S.K., Zhang, W., Subramanian, S., 2016. Characterization and cytotoxic activity of apoptosis-inducing pierisin-5 protein from white cabbage butterfly. Int. J. Biol. Macromol. 87, 16–27. https://doi.org/10.1016/j.ijbiomac.2016.01.072. Epub 2016 Jan 23 PMID: 26812112.

Suresh, K., Verma, E.J., Pritam Kumar, P., Arun Thirumurugan, S.K.S., Parashar, S.P., Mrutyunjay, S., 2018. Mechanistic Insight into Size-Dependent Enhanced Cytotoxicity of Industrial Antibacterial Titanium Oxide Nanoparticles on Colon Cells Because of Reactive Oxygen Species Quenching and Neutral Lipid Alteration. ACS Omega 3 (1), 1244–1262. https://doi.org/10.1021/acsomega.7b01522.

Tabassi, N.R., Ghasemiyan, R., Brandkam, M.R., et al, 2021. Green Synthesis of TiFe2O4@Ag Nanocomposite Using Spirulina platensis; Characterization of Their Anticancer Activity and Evaluation of Their Effect on the Expression of Bax, p53, and Bcl-2 Genes in AGS cell line. J. Clust. Sci. https://doi.org/10.1007/s10876-021-02083-8.

Tatarinov, D.A., Sokolnikova, S.R., Myslitskaya, N.A., 2021. Applying of chitosan-TiO$_2$ nanocomposites for photocatalytic degradation of anthracene and pyrene. J. Biomed. Photonics Eng. 7, 010301.

Terwilliger, T., Abdul-Hay, M., 2017. Acute lymphoblastic leukemia: a comprehensive review and 2017 update. Blood Cancer J. 7 (6), 577. https://doi.org/10.1038/bcj.2017.53. PMID: 28665419; PMCID: PMC5520400.

Vinhas, R., Mendes, R., Fernandes, A.R., Baptista, P.V., 2017. Nanoparticles-Emerging Potential for Managing Leukemia and Lymphoma. Front. Bioeng. Biotechnol. 18 (5), 79. https://doi.org/10.3389/fbioe.2017.00079. PMID: 29326927; PMCID: PMC5741836.

Yan, D., Xue, Z., Li, S., Zhong, C., 2021. Comparison of cytotoxicity of Ag/ZnO and Ag@ZnO nano complexes to human umbilical vein endothelial cells in vitro. J. Appl. Toxicol. 41 (5), 811–819. https://doi.org/10.1002/jat.4125. Epub 2020 Dec 13 PMID: 33314238.

Yang, Z.-Y., Zhong, Y.-Y., Zheng, J., Liu, Y., Li, T., Hu, E., Xiao-Fei, Z.u., Ruo-qi, D., Yao, W.u., Yi, Z., Tao, T., Feng, H.e., Shun-shun, W., Yang, W., 2021. Fmoc-amino acid-based hydrogel vehicle for delivery of amygdalin to perform neuroprotection. Smart Mat. Med. 2, 56–64. https://doi.org/10.1016/j.smaim.2020.10.004.